Dynamic modeling and design optimization of a 3-DOF spherical parallel manipulator

CrossMark

Guanglei Wu [a], Stéphane Caro [b], Shaoping Bai [a,*], Jørgen Kepler [a]

[a] *Department of Mechanical and Manufacturing Engineering, Aalborg University, DK-9220 Aalborg, Denmark*
[b] *CNRS, Institut de Recherche en Communications et Cybernétique de Nantes, UMR CNRS n° 6597, 44321 Nantes, France*

HIGHLIGHTS

- A dynamic model is derived by considering the motion characteristics of spherical parallel manipulators (SPMs).
- A comprehensive multiobjective optimization approach is formulated for SPMs.
- A Pareto-front is obtained to show the Pareto optimal solutions for selected design criteria.
- A scatter matrix is generated to show the inter-dependencies between the decision variables.

ARTICLE INFO

ABSTRACT

This paper deals with the dynamic modeling and design optimization of a three Degree-of-Freedom spherical parallel manipulator. Using the method of Lagrange multipliers, the equations of motion of the manipulator are derived by considering its motion characteristics, namely, all the components rotating about the center of rotation. Using the derived dynamic model, a multiobjective optimization problem is formulated to optimize the structural and geometric parameters of the spherical parallel manipulator. The proposed approach is illustrated with the design optimization of an unlimited-roll spherical parallel manipulator with a main objective to minimize the mechanism mass in order to enhance both kinematic and dynamic performances.

1. Introduction

The design of three Degree-of-Freedom (3-DOF) spherical parallel manipulators (SPMs) can consider many criteria, such as workspace [1–3], dexterity [4–6], dynamics [7], singularity avoidance [8], stiffness [9,10]. These evaluation criteria can be classified into two groups: one relates to the kinematic performance while the other relates to the kinetostatic/dynamic performance of the manipulator [11]. Most of the SPMs find their applications as orienting devices, such as camera orienting and medical instrument alignment [12,13], therefore, the kinematic aspects, mainly, workspace and dexterity, were extensively studied in the literature. On the other hand, the dynamics received less attention. Staicu [7] used the principle of virtual work to derive the inverse

dynamics of the Agile Wrist [10], in which recursive matrix relations for kinematics and dynamics were established. When the SPMs are used to build active spherical manipulators, for instance, wrist joint [14], the dynamic characteristics are of importance in their design and applications.

This work develops a dynamic model with the classical approach of Lagrange multipliers, which takes all the mobile components into consideration to calculate the power consumption effectively. The equations of motion for the SPMs are modeled with the motion characteristics, namely, all the bodies rotating about a fixed point (center of rotation). The derived dynamic model can be used either to assess the dynamic performance or in the design optimization.

In general, a robot design process has to simultaneously deal with the kinematic and kinetostatic/dynamic aspects, both of which include a number of performance measures that essentially vary throughout the workspace. This can be effectively achieved by virtue of multiobjective optimization method. The multiobjective optimization problems of parallel manipulators (PMs) have been reported in the literature, where various approaches of

* Corresponding author. Tel.: +45 9940 9291; fax: +45 9940 7110.
E-mail addresses: gwu@m-tech.aau.dk (G. Wu),
Stephane.Caro@irccyn.ec-nantes.fr (S. Caro), shb@m-tech.aau.dk (S. Bai),
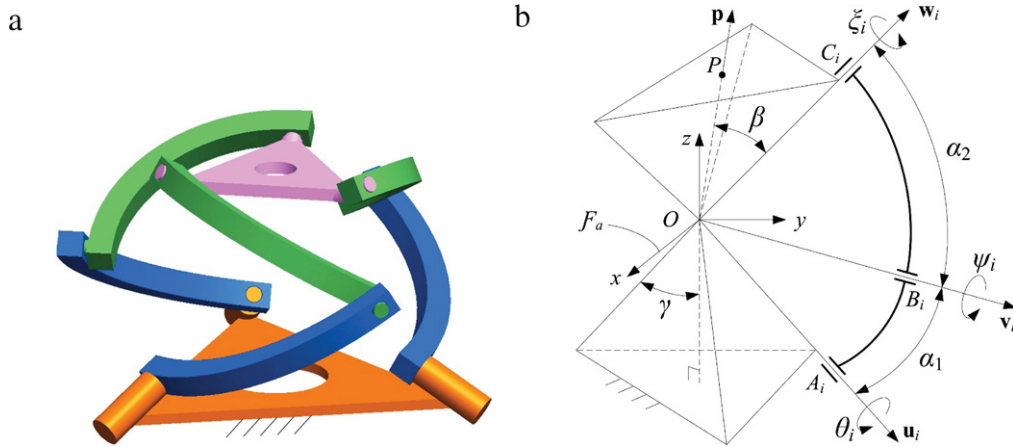jk@m-tech.aau.dk (J. Kepler).

a

b

Fig. 1. Architecture of a general SPM: (a) overview, (b) parameterization of the ith leg.
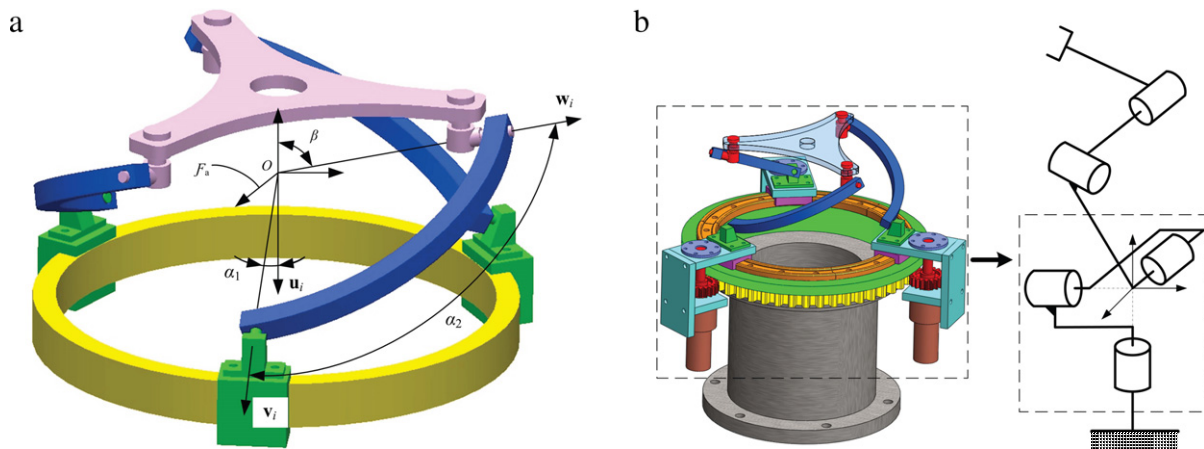
a

b

Fig. 2. (a) 3-DOF unlimited-roll SPM, which is a special case of the general SPM with $\gamma = 0$; (b) its application as spherically actuated joint.

multiobjective optimization have been applied to different types of PMs, while considering kinematic, dynamic and static criteria [11, 15–18]. However, a systematic approach lacks in the optimum design for this class of SPMs, as the static/dynamic performance received relatively less attention as mentioned above.

This paper focuses on the dynamic modeling and design optimization of the SPMs. A dynamic model of the SPM is derived based on the Lagrange equations. Based on the dynamics, together with the kinematics and stiffness of the manipulator, a multiobjective design optimization method is proposed for SPMs, aiming to formulate a general approach for the SPMs in the early design stage. The multi-objective design optimization problem is applied to a 3-DOF unlimited-roll SPM, for which the Pareto-optimal solutions are obtained with a genetic algorithm.

2. Architecture of SPMs

A general spherical parallel manipulator is shown in Fig. 1. The ith leg consists of three revolute joints, whose axes are parallel to the unit vectors $\mathbf{u}_i$, $\mathbf{v}_i$, and $\mathbf{w}_i$. All three legs have identical architectures, defined by angles $\alpha_1, \alpha_2, \beta$ and γ, where β and γ define the geometry of two regular pyramids of the base and mobile platforms. Both the two platforms are assumed to be rigid. The origin O of the base coordinate system $\mathcal{F}_a$ is located at the center of rotation. The z axis is normal to the bottom surface of the base pyramid and points upwards, while the y axis is located in the plane spanned by the z axis and $\mathbf{u}_1$ vector.

The SPM under study is a special case of $\gamma = 0$ [3], where the pyramids of the base platform is degenerated to a line segment, as shown in Fig. 2(a). The axes of the three active revolute joints are coincident with the z axis and it consists only of three curved links connected to its mobile platform. The links are driven by actuators moving independently on a circular guide via pinion and gear-ring transmissions, which can replace the serial chains based wrist mechanisms as displayed Fig. 2(b).

3. Dynamic modeling of SPMs

The orientation of the mobile platform (MP) is described by the *azimuth–tilt–torsion* $(\phi\text{–}\theta\text{–}\sigma)$ angles [19] as displayed in Fig. 3, for which the rotation matrix is expressed as:

$$\mathbf{Q} = \mathbf{R}_z(\phi)\mathbf{R}_y(\theta)\mathbf{R}_z(\sigma - \phi) \tag{1}$$

where $\phi \in (-\pi, \pi], \theta \in [0, \pi), \sigma \in (-\pi, \pi]$.

Under the prescribed coordinate system, unit vector $\mathbf{u}_i$ is derived as

$$\mathbf{u}_i = \begin{bmatrix} -\sin\eta_i \sin\gamma & \cos\eta_i \sin\gamma & -\cos\gamma \end{bmatrix}^T \tag{2}$$

where $\eta_i = 2(i-1)\pi/3, i = 1, 2, 3$.

Unit vector $\mathbf{v}_i$ of the axis of the intermediate revolute joint in the ith leg is expressed as:

$$\mathbf{v}_i = \begin{bmatrix} -s\eta_i s\gamma c\alpha_1 + (c\eta_i s\theta_i - s\eta_i c\gamma c\theta_i)s\alpha_1 \\ c\eta_i s\gamma c\alpha_1 + (s\eta_i s\theta_i + c\eta_i c\gamma c\theta_i)s\alpha_1 \\ -c\gamma c\alpha_1 + s\gamma c\theta_i s\alpha_1 \end{bmatrix} \tag{3}$$
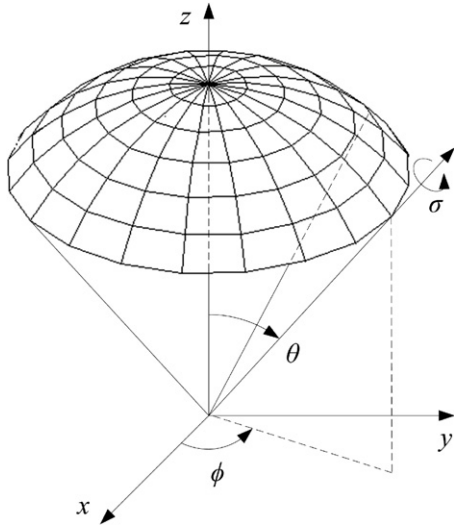
Fig. 3. Orientation representation of the *azimuth–tilt–torsion* angles.

Unit vector $\mathbf{w}_i$ of the top revolute joint in the ith leg, is a function of the orientation of the mobile platform described as

$$\mathbf{w}_i = \begin{bmatrix} w_{ix} & w_{iy} & w_{iz} \end{bmatrix}^T = \mathbf{Q}\mathbf{w}_i^* \qquad (4)$$

where $\mathbf{w}_i^*$ is the unit vector for the axis of the top revolute joint of the ith leg when the mobile platform (MP) reaches its home configuration, i.e., the MP orientation in the reference frame, which is given as

$$\mathbf{w}_i^* = \begin{bmatrix} -\sin\eta_i \sin\beta & \cos\eta_i \sin\beta & \cos\beta \end{bmatrix}^T \qquad (5)$$

3.1. Kinematic Jacobian matrix

The relationship between the angular velocity of the mobile platform $\boldsymbol{\omega} = [\omega_x\ \omega_y\ \omega_z]^T$ and the input angle velocity $\dot{\boldsymbol{\theta}} = [\dot{\theta}_1\ \dot{\theta}_2\ \dot{\theta}_3]^T$ is expressed as

$$\mathbf{A}\boldsymbol{\omega} = \mathbf{B}\dot{\boldsymbol{\theta}} \qquad (6)$$

with

$$\mathbf{A} = \begin{bmatrix} \mathbf{a}_1 & \mathbf{a}_2 & \mathbf{a}_3 \end{bmatrix}^T; \quad \mathbf{a}_i = \mathbf{v}_i \times \mathbf{w}_i \qquad (7a)$$

$$\mathbf{B} = \text{diag} \begin{bmatrix} b_1 & b_2 & b_3 \end{bmatrix}; \quad b_i = (\mathbf{u}_i \times \mathbf{v}_i) \cdot \mathbf{w}_i \qquad (7b)$$

where matrices $\mathbf{A}$ and $\mathbf{B}$ are named the forward and inverse Jacobian matrices of the manipulator, respectively. The kinematic Jacobian matrix $\mathbf{J}$ of the manipulator [1] is obtained as

$$\mathbf{J} = \mathbf{B}^{-1}\mathbf{A} = \begin{bmatrix} \mathbf{j}_1 & \mathbf{j}_2 & \mathbf{j}_3 \end{bmatrix}^T; \quad \mathbf{j}_i = \mathbf{a}_i/b_i \qquad (8)$$

3.2. Inverse dynamic modeling

The motions of the SPM bodies are shown in Fig. 4. The relationship between the angle rates $\dot{\boldsymbol{\varphi}} = [\dot{\phi}\ \dot{\theta}\ \dot{\sigma}]^T$ and the angular velocity $\boldsymbol{\omega}$ is found as [20]:

$$\begin{bmatrix} \omega_x \\ \omega_y \\ \omega_z \end{bmatrix} = \begin{bmatrix} -s\theta c\phi & -s\phi & s\theta c\phi \\ -s\theta s\phi & c\phi & s\theta s\phi \\ 1-c\theta & 0 & c\theta \end{bmatrix} \begin{bmatrix} \dot{\phi} \\ \dot{\theta} \\ \dot{\sigma} \end{bmatrix} \quad \text{or} \quad \boldsymbol{\omega} = \boldsymbol{\Phi}\dot{\boldsymbol{\varphi}} \qquad (9)$$

The dynamics of the SPM can be solved by using the Lagrange equations [21] below

$$\frac{d}{dt}\left(\frac{\partial L}{\partial \dot{\mathbf{q}}}\right) - \frac{\partial L}{\partial \mathbf{q}} + \mathbf{C}_q^T \boldsymbol{\lambda} = \mathbf{Q}_{ex} \qquad (10)$$
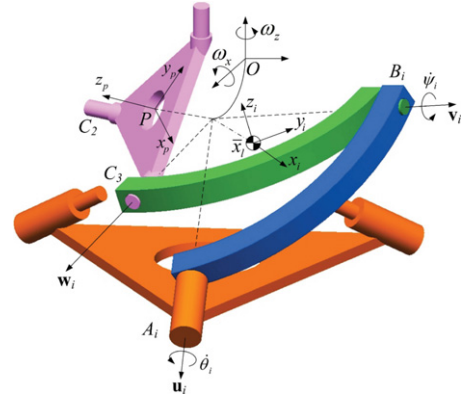

Fig. 4. The movements of the mobile platform and a single leg.

where $L \equiv T - V$ is the Lagrangian of the system, including the mobile platform and the three legs, and $\mathbf{q} = [\theta_1, \theta_2, \theta_3, \phi, \theta, \sigma]^T$. Moreover, $\mathbf{Q}_{ex} = [\boldsymbol{\tau}^T, \mathbf{0}]^T \in \mathbb{R}^6$ is the vector of external forces and vector $\boldsymbol{\tau} = [\tau_1, \tau_2, \tau_3]^T$ characterizes the actuator torques. Matrix $\mathbf{C}_q$ is the system's constraint Jacobian, which can be found from the velocity Eq. (6), namely,

$$\mathbf{B}\dot{\boldsymbol{\theta}} - \mathbf{A}\boldsymbol{\omega} = \begin{bmatrix} \mathbf{B} & -\mathbf{A}\boldsymbol{\Phi} \end{bmatrix} \begin{bmatrix} \dot{\boldsymbol{\theta}}^T & \dot{\boldsymbol{\varphi}}^T \end{bmatrix}^T = \mathbf{0} \qquad (11)$$

therefore, the matrix of constraints is found as $\mathbf{C}_q = [\mathbf{B}\ -\mathbf{A}\boldsymbol{\Phi}]$. Moreover, $\boldsymbol{\lambda} = [\lambda_1, \lambda_2, \lambda_3]^T$ is a vector of Lagrange multipliers.

3.2.1. Lagrangian of the mobile platform

The local frame (x_p, y_p, z_p) attached to the MP is established with the origin located at point P, i.e., the center of mass of the MP. Henceforth, the Lagrangian of the mobile platform is obtained as

$$L_p = T_p - V_p = \frac{1}{2}\boldsymbol{\omega}^T \mathbf{I}_p \boldsymbol{\omega} - m_p R \cos\beta \mathbf{g}^T \mathbf{p} \qquad (12)$$

where $\mathbf{I}_p$ denotes the global inertia tensor of the mobile platform, which can be found in Appendix A. Moreover, $\mathbf{g} = [0, 0, 9.81\ \text{m/s}^2]^T$.

3.2.2. Lagrangian of a single leg

The velocity $\dot{\psi}$ of the intermediate joint in ith leg is found using the following equation

$$\boldsymbol{\omega} = \dot{\theta}_i \mathbf{u}_i + \dot{\psi}_i \mathbf{v}_i + \dot{\xi}_i \mathbf{w}_i \qquad (13)$$

To eliminate $\dot{\theta}_i$ and $\dot{\xi}_i$, dot-multiplying Eq. (13) on both sides with $\mathbf{u}_i \times \mathbf{w}_i$ yields

$$(\mathbf{u}_i \times \mathbf{w}_i) \cdot \boldsymbol{\omega} = \dot{\psi}(\mathbf{u}_i \times \mathbf{w}_i) \cdot \mathbf{v}_i \quad \text{or} \quad \dot{\psi} = \mathbf{j}_{\psi i}^T \boldsymbol{\omega}$$

$$= \frac{(\mathbf{u}_i \times \mathbf{w}_i)^T}{(\mathbf{u}_i \times \mathbf{w}_i) \cdot \mathbf{v}_i}\boldsymbol{\omega} \qquad (14)$$

The angular velocity of the distal link in the ith leg in the reference frame (x, y, z) is found as $\boldsymbol{\varpi}_i = \dot{\theta}_i \mathbf{u}_i + \dot{\psi}_i \mathbf{v}_i$. Let $\boldsymbol{\varpi}_{li}$ denote the corresponding angular velocity in the local frame (x_i, y_i, z_i), we have

$$\boldsymbol{\varpi}_i = \begin{bmatrix} \mathbf{e}_{ix} & \mathbf{e}_{iy} & \mathbf{e}_{iz} \end{bmatrix} \boldsymbol{\varpi}_{li} \quad \text{or} \quad \boldsymbol{\varpi}_i = \mathbf{E}_i \boldsymbol{\varpi}_{li} \qquad (15)$$

with

$$\mathbf{e}_{ix} = \frac{\mathbf{v}_i + \mathbf{w}_i}{\|\mathbf{v}_i + \mathbf{w}_i\|}, \qquad \mathbf{e}_{iy} = \frac{\mathbf{v}_i - \mathbf{w}_i}{\|\mathbf{v}_i - \mathbf{w}_i\|}, \qquad \mathbf{e}_{iz} = \frac{\mathbf{v}_i \times \mathbf{w}_i}{\|\mathbf{v}_i \times \mathbf{w}_i\|} \qquad (16)$$

From Eq. (15), we have $\boldsymbol{\varpi}_{li} = \mathbf{E}_i^T \boldsymbol{\varpi}_i$. The Lagrangian of the ith leg is derived as below

$$L_i = T_i - V_i = \frac{1}{2}I_{l1}\dot{\theta}_i^2 + \frac{1}{2}\boldsymbol{\varpi}_i^T \mathbf{I}_{l2} \boldsymbol{\varpi}_i - m_{l1}\bar{x}_1 \mathbf{g}^T \mathbf{h}_i - m_{l2}\bar{x}_2 \mathbf{g}^T \mathbf{e}_{ix} \qquad (17)$$

where I_{l1} is the proximal link's mass moment of inertia about $\mathbf{u}_i$, and $\mathbf{I}_{l2}$ is the distal link's mass moment of inertia about point O. Moreover, $\bar{x}_1$ and $\bar{x}_2$ indicate the centers of the mass of the proximal and distal links, respectively, and $\mathbf{h}_i = (\mathbf{u}_i + \mathbf{v}_i)/\|\mathbf{u}_i + \mathbf{v}_i\|$. The details for a curved link can be found in Appendix A.

Substituting the Lagrangian L_p and L_i, $i = 1, 2, 3$, into Eq. (10), the terms in the equation of motion for this dynamic system [21] can be derived. With an external moment vector $\mathbf{m}$, the actuator torques are expressed as:

$$\boldsymbol{\tau}_a = \boldsymbol{\tau} - \mathbf{J}^{-T}\mathbf{m} \tag{18}$$

This developed dynamic model can effectively compute the active forces/torques as it takes into account all the mobile components and external forces/moments. Compared to Staicu's work [7], the model developed in this work has a more compact form, which takes advantages of the unique feature of SPMs that involves only rotations. Such a formulation can be easily understood and implemented.

4. Optimization problem of the SPMs design

The foregoing derived dynamic model can be applied in the optimization procedure to obtain a design with optimal dynamic performance. Henceforth, this section formulates a design optimization problem for the SPMs based on their dynamic modeling. Besides, the kinematic and elastic performances are also employed to evaluate the SPM design. A predefined workspace is specified as a minimum pointing cone of 90° opening with 360° full rotation, i.e., $\theta \in [0, \theta_{\min}]$, $\theta_{\min} \geq 45°$, $\{\phi, \sigma\} \in (-180°, 180°)$.

4.1. Design variables

Variables α_1, α_2 and β are part of the geometric parameters of the SPM under study. Moreover, the radius R of the link midcurve and the side length a of a square cross section of the uniform curved links are included as design parameters as well. This implies that the curved link does not include details such as slots that may affect the total mass and structural strength [22]. As a consequence, the design variables of the optimization problem at hand are:

$$\mathbf{x} = [\alpha_1, \alpha_2, \beta, a, R] \tag{19}$$

4.2. Objective functions

The mechanism mass influences the dynamic performance, such as inertia, acceleration, etc., hence, minimizing the mass of moving bodies is one important consideration. The mass m_{spm} of the SPM includes the mass m_p of the platform, the mass m_l of the distal links, and the mass m_s of the sliding units (or proximal links). The mass of the revolute joints is not considered for simplification, thus, the mass function is given as:

$$m_{spm} = m_p + 3m_l + 3m_s \tag{20}$$

As a result, the first objective function of the optimization problem is written as:

$$f_1(\mathbf{x}) = m_{spm} \rightarrow \min \tag{21}$$

The dexterity of SPMs is another major concern in the manipulator design. A commonly used criterion to evaluate this kinematic performance is the global conditioning index (GCI) [4], which describes the isotropy of the kinematic performance. The GCI is defined over a workspace Ω, which is calculated through a discrete approach in practice, namely,

$$\text{GCI} = \frac{\int_\Omega \kappa^{-1}(\mathbf{J})\mathrm{d}W}{\int_\Omega \mathrm{d}W} \quad \text{or} \quad \text{GCI} = \frac{1}{n}\sum_{k=1}^{n}\frac{1}{\kappa_k(\mathbf{J})} \tag{22}$$

where $\kappa(\mathbf{J})$ is the condition number of the kinematic Jacobian matrix (8) and $n = n_1 n_2 n_3$ is the number of the workspace points, n_1, n_2, n_3 being the numbers of discrete points along ϕ, θ, σ, respectively. It is known that the higher the GCI, the better the performance. Hereby, the second objective function of the optimization problem is written as:

$$f_2(\mathbf{x}) = 1 - \text{GCI} = \text{MGCI} \rightarrow \min \tag{23}$$

Henceforth, a modified global conditioning index (MGCI) is introduced for the purpose of optimization.

4.3. Optimization constraints

In this section, the kinematic constraints, condition number of the kinematic Jacobian matrix, elastic and dynamic performances of the manipulator are considered. Constraining the condition number of the Jacobian matrix aims to obtain a dexterous workspace free of singularity. Moreover, the constraints on the link strength and the actuator torque are also considered.

4.3.1. Geometric constraints

According to the determination of the design space reported in [3], the bounds of the parameters α_1, α_2 and β subject to the prescribed workspace are stated as:

$$45° \leq \alpha_1 \leq 135°, \qquad 45° \leq \alpha_2 \leq 135°, \qquad 45° \leq \beta \leq 90° \tag{24}$$

In accordance with Fig. 5, the following constraints should be satisfied to avoid any collision,

$$\theta_{ij} \geq \epsilon_\theta, \quad \forall \theta_{ij} \in \{\theta_{12}, \theta_{23}, \theta_{31}\} \tag{25a}$$

$$R \sin \alpha_1 \geq R_0 \tag{25b}$$

where $\epsilon_\theta = 10°$ and $R_0 = 0.120$ m are geometric parameters relative to the size of curved links.

4.3.2. Condition number of the kinematic Jacobian matrix

Minimizing MGCI, i.e., maximizing GCI, cannot prevent the prescribed workspace away from ill-conditioned configurations. For the design optimization to achieve a dexterous workspace, the minimum of the inverse condition number of the kinematic Jacobian matrix $\kappa^{-1}(\mathbf{J})$, based on the 2-norm, should be higher than a prescribed value throughout the workspace, say 0.1, namely,

$$\min(\kappa^{-1}(\mathbf{J})) \geq 0.1 \tag{26}$$

4.3.3. Strength constraints

The strength constraints are to ensure the SPM to produce allowable maximum point-displacement of the rotation center and angular deflection of the mobile platform subject to a given wrench. The deflections are computed by

$$\Delta\mathbf{x} = \mathbf{K}^{-1}\mathbf{w}; \qquad \Delta\mathbf{x} = \begin{bmatrix} \Delta\mathbf{p}^T & \Delta\boldsymbol{\varphi}^T \end{bmatrix}^T, \quad \mathbf{w} = \begin{bmatrix} \mathbf{0} & \mathbf{m}^T \end{bmatrix}^T \tag{27}$$

where $\Delta\mathbf{p} = [\Delta x, \Delta y, \Delta z]^T$ and $\Delta\boldsymbol{\varphi} = [\Delta\varphi_x, \Delta\varphi_y, \Delta\varphi_z]^T$ are the translational and rotational displacements, respectively, and $\mathbf{K}$ is the Cartesian stiffness matrix given in Appendix B. Let the static torque of the SPM within the range $\mathbf{m} = [\pm m_{x,\max}, \pm m_{y,\max}, \pm m_{z,\max}]$, the strength constraints can be written as:

$$-\epsilon_p \leq \Delta t \leq \epsilon_p, \quad \forall \Delta t \in \{\Delta x_k, \Delta y_k, \Delta z_k\} \tag{28a}$$

$$-\epsilon_r \leq \Delta r \leq \epsilon_r, \quad \forall \Delta r \in \{\Delta\varphi_{x,k}, \Delta\varphi_{y,k}, \Delta\varphi_{z,k}\} \tag{28b}$$

where ϵ_p and ϵ_r are acceptable translational and rotational errors, respectively, and $k = 1, \ldots, n$ is the number of the discrete points defined in Eq. (22).
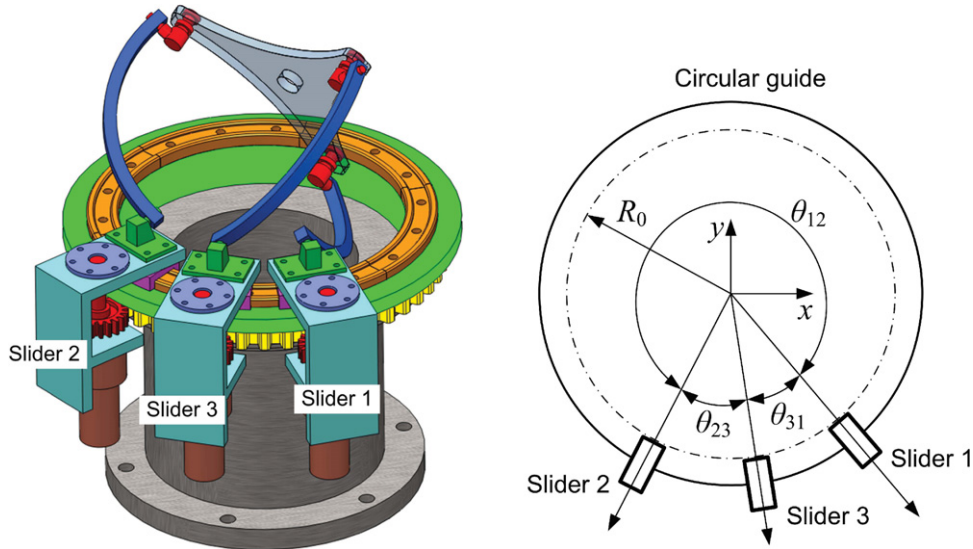
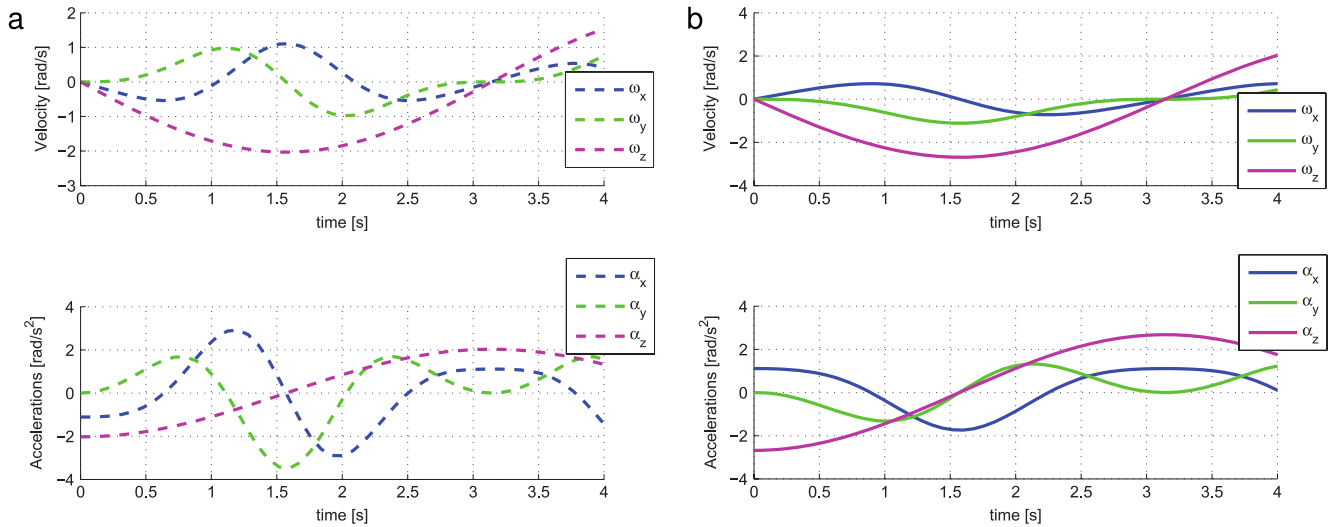**Fig. 5.** One extreme configuration of the sliding units.

Fig. 6. The angular velocity and acceleration profiles of the mobile platform: (a) trajectory 1; (b) trajectory 2.

It is noted that the model in Eq. (27) includes only the compliances of curved links. The base and MP are considered rigid. Moreover, the joint compliance is not addressed in this paper, as revolute joints are not easily characterized by a generic representative stiffness due to the nonlinear kinematic joint stiffness upon the specific design. Such an issue could be well addressed through stiffness modeling researches.

4.3.4. Actuation torque constraints

With an external moment $\mathbf{m} = [m_x, m_y, m_z]^T$ applied on the MP, in accordance to Eq. (18), the actuator torques are redefined as: $\boldsymbol{\tau}_a = |\boldsymbol{\tau}| + |\mathbf{J}^{-T}\mathbf{m}|$. At any time, the components of the actuator torque vector $\boldsymbol{\tau}_a$ should be smaller than the maximum continuous torque $T_{\max}$ of each actuator. As a result, the actuation torque constraints can be written as:

$$\max\{\boldsymbol{\tau}_a\} \leq T_{\max} \tag{29}$$

Henceforth, two alternative trajectories describing the MP orientation:

$$(1)\ \phi(t) = \pi \cos t, \qquad \theta(t) = \frac{\pi}{4}, \qquad \sigma(t) = \frac{\pi}{2} \cos t \tag{30}$$

$$(2)\ \phi(t) = \frac{\pi}{2} \cos t, \qquad \theta(t) = \frac{\pi}{4}, \qquad \sigma(t) = \pi \cos t$$

are integrated into the optimization procedure implemented with the *Matlab/simulink* package. The corresponding angular velocity and acceleration profiles of the mobile platform are shown in Fig. 6.

4.4. Formulation of the multi-objective design optimization problem

The multi-objective design optimization problem for the SPM is formulated as:

$$\text{minimize} \quad f_1(\mathbf{x}) = m_{spm} \tag{31}$$

$$\text{minimize} \quad f_2(\mathbf{x}) = MGCI$$

$$\text{over} \quad \mathbf{x} = [\alpha_1;\ \alpha_2;\ \beta;\ a;\ R]$$

$$\text{subject to} \quad g_1 : R\sin\alpha_1 \geq R_0$$

$$g_2 : \theta_{ij} \geq \epsilon_\theta, \quad \forall \theta_{ij} \in \{\theta_{12},\ \theta_{23},\ \theta_{31}\}$$

$$g_3 : \theta_{\min} \geq 45°$$

$$g_4 : \min(\kappa^{-1}(\mathbf{J})) \geq 0.1$$

$$g_5 : -\epsilon_p \leq \Delta t \leq \epsilon_p, \quad \forall \Delta t \in \{\Delta x_k,\ \Delta y_k,\ \Delta z_k\}$$

$$g_6 : -\epsilon_r \leq \Delta r \leq \epsilon_r, \quad \forall \Delta r \in \{\Delta\varphi_{x,k},\ \Delta\varphi_{y,k},\ \Delta\varphi_{z,k}\}$$
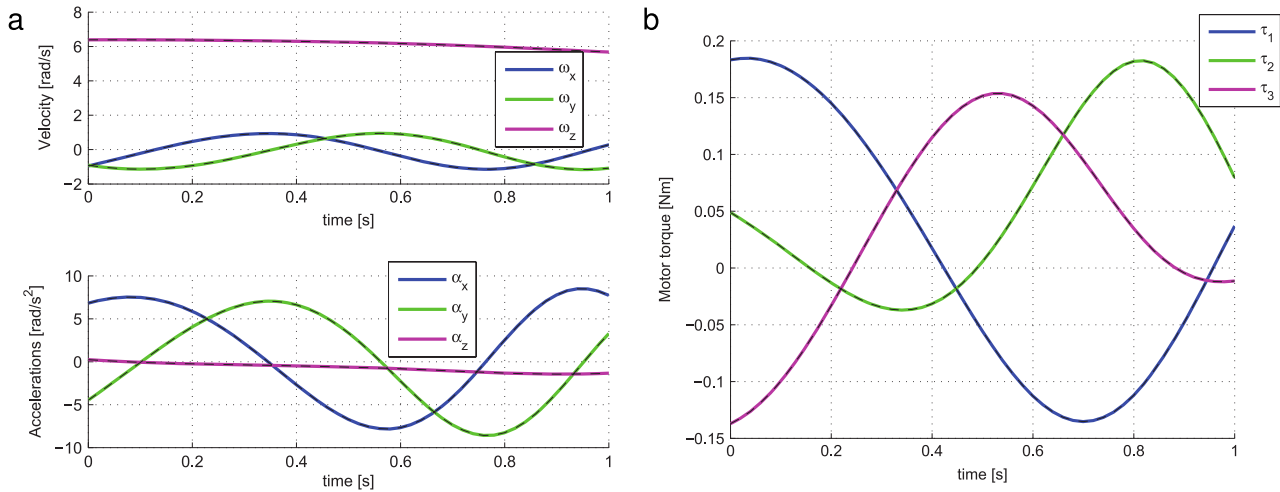
$$g_7 : \max\{\boldsymbol{\tau}_a\} \leq T_{\max}$$

Fig. 7. Simulation results (solid line stands for Matlab solver, dashed line for Adams): (a) motion of the mobile platform; (b) actuator torques.

Table 1
Parameters of the SPM and the initial simulation condition.

α_1 (deg)	α_2 (deg)	β (deg)	$[\phi, \theta, \sigma]$ (rad)	$[\dot{\theta}_1, \dot{\theta}_2, \dot{\theta}_3]$ (rad/s)	$\mathbf{m}$ (N m)
60	75	75	$[0, \pi/6, 0]$	$[-6, -5, -7]$	$[0.1, 0.1, 0.1]$

Table 2
Mass and inertia properties of the SPM model.

Mobile platform		Curved link		Sliding unit
m_p (kg)	$\mathbf{I}_p$ (10^{-4} kg m^2)	m_l (kg)	$\mathbf{I}_l$ (10^{-4} kg m^2)	m_s (kg)
0.332	[3.855 3.855 7.688]	0.107	[1.816 0.081 1.894]	0.123

5. Results and discussion

5.1. Validation of dynamic model

Dynamic simulations were conducted with the developed SPM dynamic model, the obtained results being compared with those obtained with *MSC Adams*, utilizing the properties and simulation conditions given in Tables 1 and 2. The corresponding simulation results from the developed model and the Adams simulation are shown in Fig. 7, which shows a good agreement with each other.

5.2. Design optimization

The optimization procedure is applied to the SPM shown in Fig. 2(b). The actuation transmission mechanism is a combination of RE 35 GB actuator and GP 42 C gearhead from Maxon [23]. The components are supposed to be made up of steel, and the mobile platform is supposed to be a regular triangle. The total mass m_s of each slide unit, including the mass of the actuator, gearhead, pinions and the manufactured components, is equal to $m_s = 2.1$ kg. Henceforth, the actuation stiffness is $K_{act}^i = 10^6$ N m/rad and the range of the static moment in Eq. (27) is $\mathbf{m} = [\pm 10, \pm 10, \pm 10]$ N m, while the acceptable translational and rotational errors are $\epsilon_p = 1$ mm and $\epsilon_r = 0.0349$ rad, respectively. Moreover, the maximum continuous torque of the actuator is $T_{max} = 15$ N m and the external moment applied on the mobile platform and expressed in the base frame along the trajectories defined by Eq. (30) is $\mathbf{m} = [5, 5, 5]^T$ N m.

The solutions of the previous optimization problem are non-dominated solutions, also called Pareto-optimal solutions, which stand for solutions for which the corresponding objectives cannot be further improved without degrading others. Problem (31) is
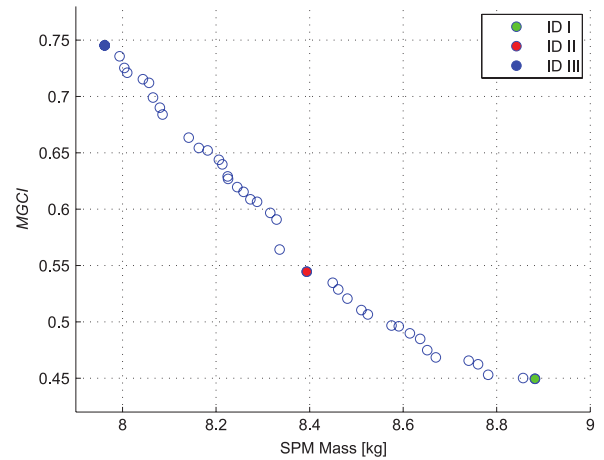

Fig. 8. The Pareto-front of the multiobjective optimization problem (31).

solved by the genetic algorithm NSGA-II [24] implemented in *Matlab*, for which the algorithm parameters are given in Table 3. The lower and upper bounds of the design variables are shown in Table 4, denoted by $\mathbf{x}_{lb}$ and $\mathbf{x}_{ub}$, respectively.

The Pareto-front of the optimization problem at hand is shown in Fig. 8. Three Pareto-optimal solutions named ID-I, ID-II and ID-III on the Pareto-fronts, i.e., two extreme solutions and one intermediate solution, described in Table 5, are selected for further consideration. The CAD designs of these three Pareto-optimal solutions are shown in Fig. 9 and the corresponding dynamic simulations are illustrated in Fig. 10, respectively, from which it is seen that from ID-I to III, the maximum actuating torque increases. By comparison among the three groups of design variables in Table 5, smaller α_1 and larger α_2 yield higher wrench capability under given input torques. Although the design ID-III has the lowest mass, it has the highest requirements on the actuators. From the kinematic and dynamic considerations, design ID-I can be selected for further application as an active joint.

Fig. 11, obtained with *plotmatrix* and *corrcoef* functions in *Matlab*, illustrates the variational trends as well as the inter-dependency between the objective functions and design variables by means of a scatter matrix [11,18]. The lower triangular part of the matrix represents the correlation coefficients whereas the upper one shows the corresponding scatter plots. The diagonal elements represent the probability density charts of each variable. The correlation coefficients vary from -1 to 1. Two variables are
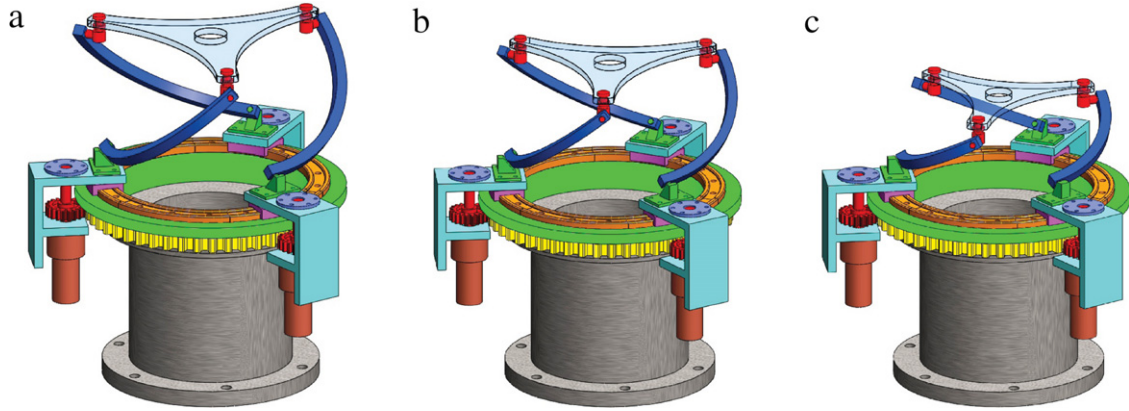
Fig. 9. CAD designs of three Pareto-optimal solutions: (a) ID-I, (b) ID-II, (c) ID-III.

Table 3
Algorithm parameters of the implemented NSGA-II.

Population size	Number of generations	Directional crossover probability	Crossover probability	Distribution index
40	200	0.5	0.9	20

Table 4
The lower and upper bounds of the design variables.

	α_1 (deg)	α_2 (deg)	β (deg)	a (m)	R (m)
$\mathbf{x}_{lb}$	45	45	45	0.005	0.120
$\mathbf{x}_{ub}$	135	135	90	0.030	0.300

strongly dependent when their correlation coefficient is close to −1 or 1 and independent when the latter is null. Fig. 11 shows that:

- m_{spm} and MGCI are strongly dependent as their correlation coefficient is equal to −0.984;
- m_{spm} and MGCI are strongly dependent on the design variables except a as the mass of the sliding units mainly affects the total mass, thus, a slightly affects m_{spm};
- both objective functions are approximately linearly related to variables α_1, α_2 and R;
- all the variables are strongly dependent on each other except a;
- the results show that β is close to 90° for all Pareto-optimal solutions;
- it is noteworthy that the higher m_{spm}, the lower α_1. Conversely, the higher m_{spm}, the higher α_2. Higher R results in higher m_{spm}.

6. Conclusions

In this paper, the inverse dynamics and geometric synthesis of spherical parallel manipulators were discussed. Using the classical method of Lagrange multipliers, the equations of motion for the SPMs were derived. The expressions for the kinetic energy are associated with the characteristics of motion, namely, all the SPM bodies rotating about the center of rotation. All the moving bodies are taken into account to describe this dynamic system effectively and clearly. The developed dynamic model is integrated into the design optimization procedure of the SPMs.

A multiobjective design optimization problem was formulated in order to determine the mechanism optimum structural and geometric parameters. The objective functions were evaluated based on the kinematic and kinetostatic/dynamic performances of the manipulators. This approach has been illustrated with the optimum design of an unlimited-roll spherical parallel manipulator, aiming at minimizing the mechanism mass and increasing its dexterity. As a result, the Pareto-front was obtained to show the approximation of the optimal solutions between the various (antagonistic) criteria, subject to the dependency of the performance. It turns out that the manipulator has the best performance with $\beta = 90°$.

As a matter of fact, the method offers a great flexibility to select any criterion as an objective function based on requirements. A contribution of the work is the formulation of different kinds of performances ranging from kinematics, statics to dynamics. All these formulations ease the modeling and simulation, and can be used for other design optimization tasks in future work.

Appendix A. Mass moment of inertia

The mass moment of inertia of the mobile platform about point O [25] is given by

$$\mathbf{I}_p = m_p R^2 \cos^2 \beta [\mathbf{p}]_\times [\mathbf{p}]_\times^T + \mathbf{Q}\mathbf{I}_p'\mathbf{Q}^T \tag{A.1}$$

where m_p is the mass, $\mathbf{I}_p'$ is the inertia tensor in its local frame (x_p, y_p, z_p), and $[\mathbf{p}]_\times = \mathrm{CPM}(\mathbf{p})$ is the skew-symmetric matrix, $\mathbf{p}$ being the unit vector of z_p axis in Fig. 4.

A parameterized curved link with uniform cross-section is shown in Fig. 12, its center of mass being found as

$$R\alpha\bar{x} = R^2 \int_{-\frac{\alpha}{2}}^{\frac{\alpha}{2}} \cos\varphi\,\mathrm{d}\varphi \quad \text{or} \quad \bar{x} = \frac{2R}{\alpha}\sin\frac{\alpha}{2} \tag{A.2}$$

Table 5
Three Pareto-optimal solutions.

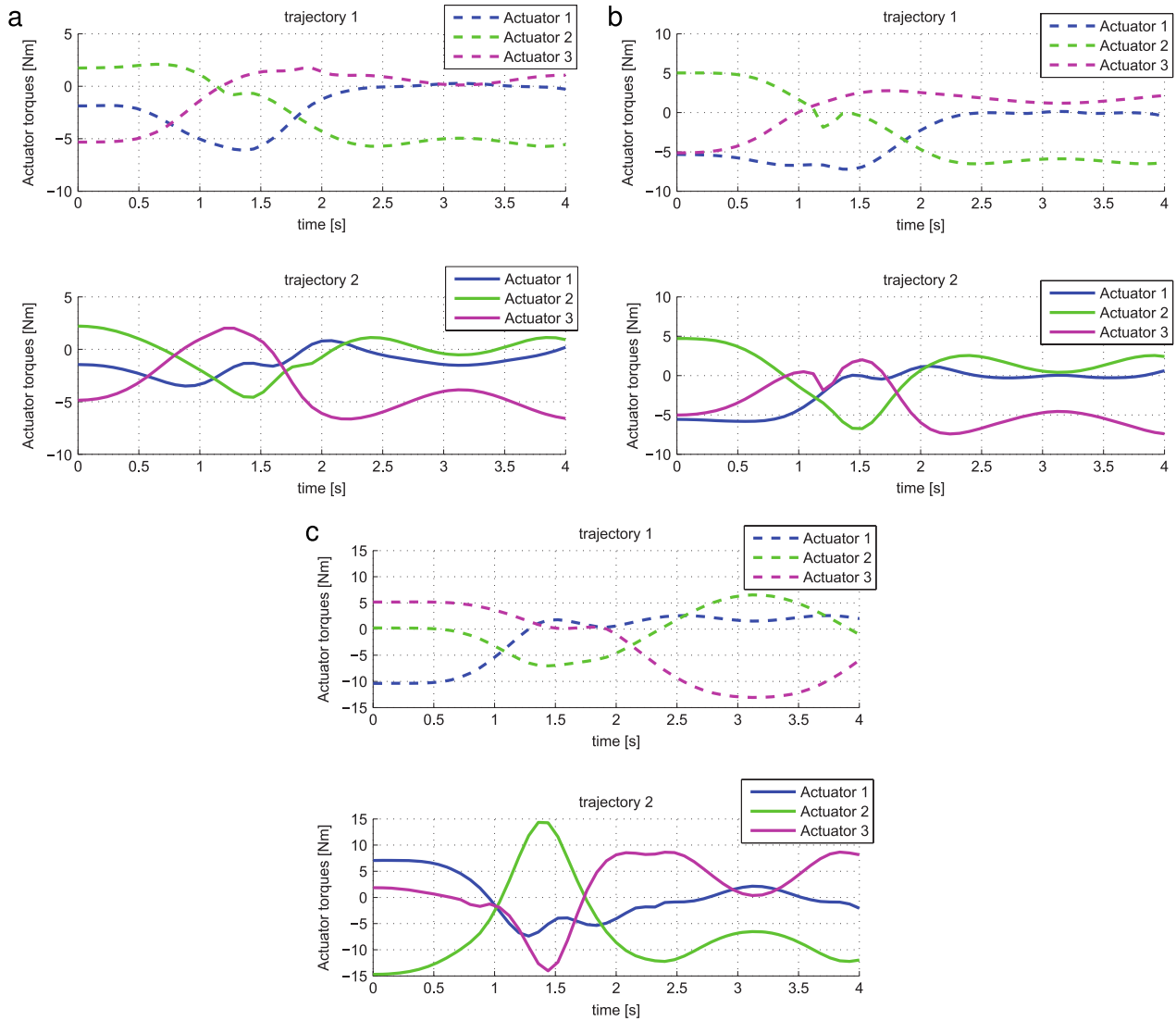| Design ID	Variables					Objectives		
	α_1 (deg)	α_2 (deg)	β (deg)	a (m)	R (m)	m_{spm} (kg)	MGCI	$\min(\kappa^{-1}(\mathbf{J}))$
I	47.2	91.7	88.4	0.0120	0.1659	8.882	0.449	0.253
II	51.9	85.0	88.3	0.0113	0.1525	8.394	0.545	0.240
III	63.5	72.2	89.6	0.0119	0.1342	7.962	0.745	0.102

Fig. 10. The dynamic simulation results for the three Pareto-optimal solutions: (a) ID-I; (b) ID-II; (c) ID-III.
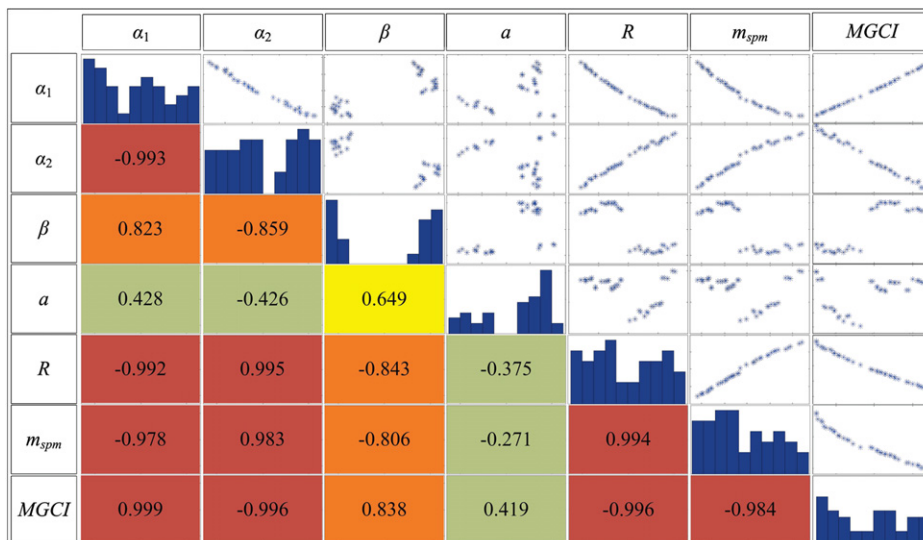

Fig. 11. Scatter matrix for the objective functions and the design variables.
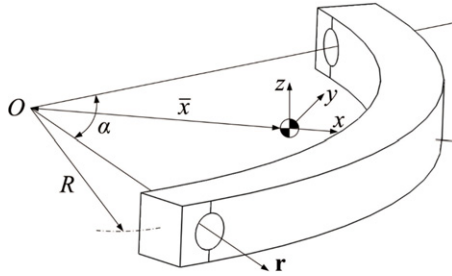
Fig. 12. A curved link.

Let the link's mass be m_l, its moment of inertia about point O is found as [25]:

$$\mathbf{I}_l = m_l \bar{x}^2 [\mathbf{i}]_\times [\mathbf{i}]_\times^T + \mathbf{E}\mathbf{I}_l'\mathbf{E}^T \tag{A.3}$$

where $[\mathbf{i}]_\times = \mathrm{CPM}(\mathbf{i})$, and $\mathbf{E} = [\mathbf{i}\ \mathbf{j}\ \mathbf{k}]$, $\mathbf{i}$, $\mathbf{j}$, $\mathbf{k}$ being the unit vectors of x, y and z-axes. Moreover, the mass moments of inertia $\mathbf{I}_l' = \mathrm{diag}[L_{xx}\ L_{yy}\ L_{zz}]$ in the frame (x, y, z) are expressed as:

$$L_{xx} = \int_{-\frac{\alpha}{2}}^{\frac{\alpha}{2}} (R\sin\varphi)^2 \cdot \frac{m_l}{R\alpha} \cdot R\mathrm{d}\varphi = \frac{1}{2}m_l R^2 \left(1 - \frac{\sin\alpha}{\alpha}\right) \tag{A.4a}$$

$$\begin{aligned} L_{yy} &= \int_{-\frac{\alpha}{2}}^{\frac{\alpha}{2}} (R\sin\varphi - \bar{x})^2 \cdot \frac{m_l}{R\alpha} \cdot R\mathrm{d}\varphi \\ &= \frac{1}{2}m_l \left(\frac{R^2\sin\alpha}{\alpha} - \frac{8R\bar{x}}{\alpha}\sin\frac{\alpha}{2} + R^2 + 2\bar{x}^2\right) \end{aligned} \tag{A.4b}$$

$$\begin{aligned} L_{zz} &= \int_{-\frac{\alpha}{2}}^{\frac{\alpha}{2}} \left[(R\sin\varphi)^2 + (R\cos\varphi - \bar{x})^2\right] \cdot \frac{m_l}{R\alpha} \cdot R\mathrm{d}\varphi \\ &= \frac{1}{2}m_l \left(R^2 + \bar{x}^2 - \frac{4R\bar{x}}{\alpha}\sin\frac{\alpha}{2}\right) \end{aligned} \tag{A.4c}$$

Moreover, the mass moment of inertia about $\mathbf{r}$ is derived as

$$\begin{aligned} I_l &= m_l \left(\bar{x}\sin\frac{\alpha}{2}\right)^2 + \int_0^\alpha (R\sin\varphi)^2 \cdot \frac{m_l}{R\alpha} \cdot R\mathrm{d}\varphi \\ &= \frac{1}{4}m_l R^2 \left[\frac{(1-\cos\alpha)^2}{\alpha^2} + 2 - \frac{\sin 2\alpha}{\alpha}\right] \end{aligned} \tag{A.5}$$

Appendix B. Cartesian stiffness matrix

With the virtual-spring approach [26], the Cartesian stiffness matrix $\mathbf{K}$ of the SPM is found as

$$\mathbf{K} = \sum_{i=1}^{3} \mathbf{K}_i \tag{B.1}$$

Here $\mathbf{K}_i \in \mathbb{R}^6$ is the Cartesian stiffness matrix of the ith leg, extracted from the first six-dimensional block of matrix $\mathbf{K}_i'$

$$\mathbf{K}_i' = \begin{bmatrix} \mathbf{J}_\theta^i (\mathbf{K}_\theta^i)^{-1}\mathbf{J}_\theta^{iT} & \mathbf{J}_q^i \\ \mathbf{J}_q^{iT} & \mathbf{0}_2 \end{bmatrix}^{-1} \tag{B.2}$$

with

$$\mathbf{J}_\theta^i = \begin{bmatrix} \hat{\mathbf{S}}_A^i & \hat{\mathbf{S}}_{u1}^i & \dots & \hat{\mathbf{S}}_{u12}^i \end{bmatrix} \in \mathbb{R}^{6\times 13} \tag{B.3a}$$

$$\mathbf{J}_q^i = \begin{bmatrix} \hat{\mathbf{S}}_B^i & \hat{\mathbf{S}}_C^i \end{bmatrix} \in \mathbb{R}^{6\times 2} \tag{B.3b}$$

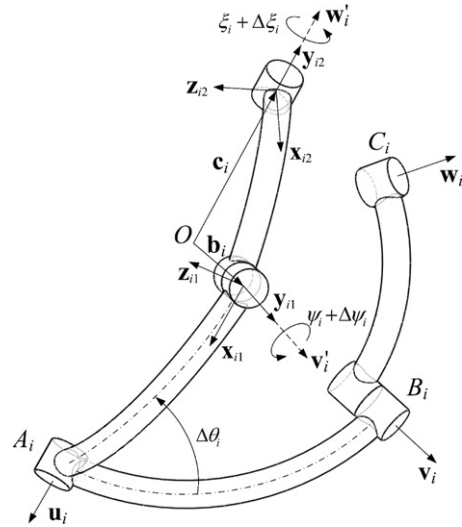**Fig. 13.** Link deflections and joint displacements of a flexible leg.

According to Fig. 13, the unit screws are given by

$$\hat{\mathbf{S}}_A^i = \begin{bmatrix} \mathbf{u}_i \\ \mathbf{0} \end{bmatrix}, \qquad \hat{\mathbf{S}}_B^i = \begin{bmatrix} \mathbf{v}_i \\ \mathbf{0} \end{bmatrix}, \qquad \hat{\mathbf{S}}_C^i = \begin{bmatrix} \mathbf{w}_i \\ \mathbf{0} \end{bmatrix}$$

$$\hat{\mathbf{S}}_{u1}^i = \begin{bmatrix} \mathbf{x}_{i1} \\ \mathbf{b}_i \times \mathbf{x}_{i1} \end{bmatrix}, \qquad \hat{\mathbf{S}}_{u2}^i = \hat{\mathbf{S}}_B^i, \qquad \hat{\mathbf{S}}_{u3}^i = \begin{bmatrix} \mathbf{z}_{i1} \\ \mathbf{b}_i \times \mathbf{z}_{i1} \end{bmatrix},$$

$$\hat{\mathbf{S}}_{u4}^i = \begin{bmatrix} \mathbf{0} \\ \mathbf{x}_{i1} \end{bmatrix}, \qquad \hat{\mathbf{S}}_{u5}^i = \begin{bmatrix} \mathbf{0} \\ \mathbf{v}_i \end{bmatrix}, \qquad \hat{\mathbf{S}}_{u6}^i = \begin{bmatrix} \mathbf{0} \\ \mathbf{z}_{i1} \end{bmatrix}$$

$$\hat{\mathbf{S}}_{u7}^i = \begin{bmatrix} \mathbf{x}_{i2} \\ \mathbf{c}_i \times \mathbf{x}_{i2} \end{bmatrix}, \qquad \hat{\mathbf{S}}_{u8}^i = \hat{\mathbf{S}}_C^i, \qquad \hat{\mathbf{S}}_{u9}^i = \begin{bmatrix} \mathbf{z}_{i2} \\ \mathbf{c}_i \times \mathbf{z}_{i2} \end{bmatrix},$$

$$\hat{\mathbf{S}}_{u10}^i = \begin{bmatrix} \mathbf{0} \\ \mathbf{x}_{i2} \end{bmatrix}, \qquad \hat{\mathbf{S}}_{u11}^i = \begin{bmatrix} \mathbf{0} \\ \mathbf{w}_i \end{bmatrix}, \qquad \hat{\mathbf{S}}_{u12}^i = \begin{bmatrix} \mathbf{0} \\ \mathbf{z}_{i2} \end{bmatrix} \tag{B.4}$$

and $\mathbf{K}_\theta^i \in \mathbb{R}^{13}$ describes the stiffness of the actuation and virtual springs, taking the form:

$$\mathbf{K}_\theta^i = \mathrm{diag}\begin{bmatrix} K_{act}^i & \mathbf{K}_{L_1}^i & \mathbf{K}_{L_2}^i \end{bmatrix} \tag{B.5}$$

where K_{act}^i is the ith actuator stiffness, $\mathbf{K}_{L_1}^i$ and $\mathbf{K}_{L_2}^i$, respectively, are the 6×6 stiffness matrices of the proximal and distal curved links in the ith leg, which can be found in [27].

References

[1] C.M. Gosselin, J. Angeles, The optimum kinematic design of a spherical three-degree-of-freedom parallel manipulator, ASME J. Mech. Transm. Autom. Des. 111 (1989) 202–207.

[2] F. Bulca, J. Angeles, P.J. Zsombor-Murray, On the workspace determination of spherical serial and platform mechanisms, Mech. Mach. Theory 34 (3) (1999) 497–512.

[3] S. Bai, Optimum design of spherical parallel manipulators for a prescribed workspace, Mech. Mach. Theory 45 (2) (2010) 200–211.

[4] C.M. Gosselin, J. Angeles, A global performance index for the kinematic optimization of robotic manipulators, ASME J. Mech. Des. 113 (3) (1991) 220–226.

[5] C.M. Gosselin, E. Lavoie, On the kinematic design of spherical three-degree-of-freedom parallel manipulators, Int. J. Robot. Res. 12 (4) (1993) 394–402.

[6] S. Bai, M.R. Hansen, T.O. Andersen, Modelling of a special class of spherical parallel manipulators with Euler parameters, Robotica 27 (2) (2009) 161–170.

[7] S. Staicu, Recursive modelling in dynamics of Agile Wrist spherical parallel robot, Robot. Comput.-Integr. Manuf. 25 (2) (2009) 409–416.

[8] I.A. Bonev, C.M. Gosselin, Singularity loci of spherical parallel mechanisms, IEEE International Conference on Robotics and Automation, Barcelona, Spain, 2005, pp. 2957–2962.

[9] X.J. Liu, Z.L. Jin, F. Gao, Optimum design of 3-DOF spherical parallel manipulators with respect to the conditioning and stiffness indices, Mech. Mach. Theory 35 (9) (2000) 1257–1267.

[10] F. Bidault, C.-P. Teng, J. Angeles, Structural optimization of a spherical parallel manipulator using a two-level approach, Proc. ASME 2001 Design Engineering Technical Conferences, Pittsburgh, Pennsylvania, 2001, pp. 9–12.
[11] S. Caro, D. Chablat, R. Ur-Rehman, P. Wenger, Multiobjective design optimization of 3-PRR planar parallel manipulators, Glob. Prod. Dev. (2011) 373–383.
[12] C.M. Gosselin, J.F. Hamel, The Agile Eye: a high-performance three-degree-of-freedom camera-orienting device, IEEE International Conference on Robotics and Automation, San Diego, CA, 1994, pp. 781–786.
[13] T. Li, S. Payandeh, Design of spherical parallel mechanisms for application to laparoscopic surgery, Robotica 20 (2) (2002) 133–138.
[14] H. Asada, J. Granito, Kinematic and static characterization of wrist joints and their optimal design, IEEE International Conference on Robotics and Automation, 1985, pp. 244–250.
[15] M. Ceccarelli, G. Carbone, E. Ottaviano, Multi criteria optimum design of manipulators, Bull. Pol. Acad. Tech. Sci. 53 (1) (2005) 9–18.
[16] O. Altuzarra, O. Salgado, A. Hernandez, J. Angeles, Multiobjective optimum design of a symmetric parallel schönflies-motion generator, ASME J. Mech. Des. 131 (3) (2009) 031002.
[17] D. Chablat, S. Caro, R. Ur-Rehman, P. Wenger, Comparison of planar parallel manipulator architectures based on a multi-objective design optimization approach, ASME 2010 International Design Engineering Technical Conferences and Computers and Information in Engineering Conference, Montreal, Quebec, Canada, 2010, pp. 861–870.
[18] R. Ur-Rehman, S. Caro, D. Chablat, P. Wenger, Multi-objective path placement optimization of parallel kinematics machines based on energy consumption, shaking forces and maximum actuator torques: Application to the Orthoglide, Mech. Mach. Theory 45 (8) (2010) 1125–1141.
[19] I.A. Bonev, Direct kinematics of zero-torsion parallel mechanisms, IEEE International Conference on Robotics and Automation, Pasadena, California, USA, 2008, pp. 3851–3856.
[20] J. Diebel, Representing attitude: Euler angles, unit quaternions, and rotation vectors, Stanford University Technical Report, Stanford University, Stanford, CA, 2006.
[21] J.G. Jalón, E. Bayo, Kinematic and Dynamic Simulation of Multibody Systems: The Real-Time Challenge, Springer-Verlag, New-York, 1994.
[22] L. Zhou, S. Bai, M.R. Hansen, Integrated dimensional and drive-train design optimization of a light-weight anthropomorphic arm, Robot. Auton. Syst. 60 (1) (2012) 113–122.
[23] Maxon products catalog (2012), http://www.maxonmotor.com/maxon/view/catalog/.
[24] K. Deb, A. Pratap, S. Agarwal, T. Meyarivan, A fast and elitist multiobjective genetic algorithm: NSGA-II, IEEE Trans. Evol. Comput. 6 (2) (2002) 182–197.
[25] J. Awrejcewicz, Z. Koruba, Equations of motion of a rigid spherical body, Adv. Mech. Math.: Class. Mech. 30 (2012) 87–123.
[26] A. Pashkevich, D. Chablat, P. Wenger, Stiffness analysis of overconstrained parallel manipulators, Mech. Mach. Theory 44 (5) (2009) 966–982.
[27] G. Wu, S. Bai, J. Kepler, Mobile platform center shift in spherical parallel manipulators with flexible limbs, Mech. Mach. Theory 75 (2014) 12–26.

Guanglei Wu received his B.Eng. in Machinery Design, Manufacturing and Automation from Yantai University, China, in 2007 and M.Eng. in Machinery Manufacturing and Automation from Northeastern University, China, in 2009. He is currently a Ph.D. Student in the Department of Mechanical and Manufacturing Engineering at Aalborg University, Denmark. His main research interest is in modeling and design of parallel manipulators.

Stéphane Caro received the Engineering and M.Sc. degrees in mechanical engineering from Ecole Centrale Nantes (ECN), Nantes, France, in 2001, and the Doctorate degree in mechanical engineering from the University of Nantes in 2004. He was a Post-doctoral Fellow in the Centre for Intelligent Machines, McGill University, Montreal, QC, Canada from 2005 to 2006. He is currently a full-time researcher of the National Centre for Scientific Research (CNRS) and works in the Research Institute in Communications and Cybernetics of Nantes (IRCCyN) and at the French Technological Research Institute (IRT) Jules Verne. His research interests include conceptual design of robots, robust design, kinematic analysis and synthesis, singularity analysis, sensitivity analysis, tolerance synthesis, and design optimization.

Shaoping Bai is an associate professor at the Department of Mechanical and Manufacturing Engineering, Aalborg University (AAU), Denmark. His research interests include medical and assistive robots, parallel manipulators, walking robots, dynamics and design.

Jørgen A. Kepler, Ph.D., is an associate professor at the Department of Mechanical and Manufacturing Engineering, Aalborg University, Denmark. His research interests include mechanical systems, impact dynamics, elasticity theory.